Human-Robot Coordination Control of Robotic Exoskeletons by Skill Transfers

Zhijun Li, *Senior Member, IEEE*, Yu Kang, *Senior Member, IEEE*, Zhiye Xiao, and Weiguo Song

***Abstract*—Neuro-motor control experiments have shown that humans are able to adapt limb impedance to stably and properly interact with various environmental forces with dexterous skills. Inspired by these observations, in this paper we develop a control approach in which the robot automatic control is combined with impedance control using stiffness transferred from human operator. Under the assumption of linear mapping between muscle surface electromyography (sEMG) signal amplitude and human arm stiffness, we employ the incremental stiffness extraction method in operational space with an improved performance by compensation of the non-linear residual error in the mapping. The teleoperated robotic exoskeleton is able to replicate the impedance of human operator's arm, and simultaneously compensate for external disturbances by the technique of disturbance observer. Experimental studies have been carried out to test the anti-disturbance ability of the proposed approach for the pose maintenance task in the presence of both stable and unstable interactive forces. The effectiveness of the proposed approach has been demonstrated by the experimental results.**

***Index Terms*—Coordination Control, Robotic Exoskeletons, Skill Transfers**

I. Introduction

ASSISTIVE robot exoskeletons can provide motion support to humans, especially be applicable to elderly people and patients with impaired motor functions who cannot generate necessary amount of forces to perform intended tasks [1], [2], [3]. On the other hand, robotic exoskeletons are also used to strength the power of healthy people and enhance their endurance for heavy tasks. As we know, humans demonstrate versatile and stable interactions with the uncertain environment, which can be achieved through the modulation of the mechanical properties of the limbs [4]. Neuromotor experimental studies have shown that the impedance of the human joints can be voluntarily adapted during motion. If the delicate impedance adaptation skills of human operator can be incorporated into robot control, it would greatly benefit the physical human-robot interaction [5].

Recently, there has been a strong interest in developing robots with inherently compliant joints [6], [7]. Partially because the introduction of muscle-like elasticity into robots help to improve their performance by intrinsically absorbing external impacts. These robots with physically compliant joints have the advantage of being safer than robots on which the compliance is achieved actively, since the robot remains compliant even in the case of sensor failures. However, most of the existing robots do not have physical elastic joints, it is thus desired to achieve compliant manipulation using control algorithms, which can be designed in various manners, depending on the task representation and control system of the robot [8]. Traditionally, the impedance regulation can be introduced to torque controlled robots to regulate actively their impedance properties by active control techniques. In [9], the compliance interaction between robot and environment was considered for mobile manipulators, by using compliance-based controls in joint coordinates or in Cartesian coordinates. A direct method has been implemented in [10] to regulate stiffness and damping properties in torque control mode using adaptive control techniques.

For human operator, limb motions are directly generated by numerous skeletal muscles associated to a certain joint. Consequently, one would expect to extract motion information by estimating the muscular contraction levels of the related joints from surface electromyography(sEMG) signals, and to further estimate joint force and stiffness, such that complete motion of the operator could be identified and recognized. However, accurate estimation based on sEMG is challenging, especially when there are multiple degree for freedom (DoF) involved. For example, one wrist joint at least involves two DoF and more than ten muscles, and consequently leads to complex interrelations. Furthermore, sEMG signals of skin surface are of several non-linear and non-stationary properties, and these signals only involve the information about surface muscles instead of all related skeletal muscles.

In this paper, we aim to set up a control framework that combines the human operated control and robot automatic control to achieve disturbance rejection. Recently, there are some works conducted to investigate the disturbance observer-based motion controllers [12], [29]. Disturbance observer-based control is of simple structure but of power to compensate for various uncertainties, but it cannot sufficiently compensate all uncertainties when the dynamics model is unknown and the perturbation is fast varying. To overcome the dynamics uncertainties, the human stiffness transfer and adaptive control techniques have been employed to achieve good performance

Manuscript received May 25, 2016; revised September 22, 2016; accepted October 30, 2016. This work is supported in part by National Natural Science Foundation of China grants Nos. 61573147, 91520201, 61625303, 61422307, 61673361, and Guangzhou Research Collaborative Innovation Projects (No. 2014Y2-00507), Guangdong Science and Technology Research Collaborative Innovation Projects under Grant Nos. 2014B090901056, 2015B020214003, Guangdong Science and Technology Plan Project (Application Technology Research Foundation) No. 2015B020233006, in part by the Scientific Research Staring Foundation for the Returned Overseas Chinese Scholars, Ministry of Education of China, in part by the national Youth Top-Notch Talent Support Program.

Z. Li is currently with College of Automation Science and Engineering, South China University of Technology, Guangzhou, and also with Department of Automation, University of Science and Technology, Hefei, China. Email:zjli@ieee.org.

Y. Kang, and W. Song are with State Key Laboratory of Fire ScienceInstitute of Advanced Technology and Department of Automation, University of Science and Technology of China, Hefei, China and with Key Laboratory of Technology in GeoSpatial Information Processing and Application System, Chinese Academy of Sciences, Beijing,China. Email: kangduyu@ustc.edu.cn.

Z. Xiao is with College of Automation Science and Engineering, South China University of Technology, Guangzhou.Email: 346222175@qq.com.

* Corresponding author: Yu Kang.

This article has been accepted for publication in a future issue of this journal, but has not been fully edited. Content may change prior to final publication. Citation information: DOI 10.1109/TIE.2016.2638403, IEEE Transactions on Industrial Electronics

in the previous works [13], [10]. However, the human stiffness transfer and adaptive control may exhibit unsatisfactory transient performance and cannot handle unparameterizable external disturbances through parameter adaptation. The combination of the disturbance observer and the human stiffness transfer and adaptive control techniques, however, has not been well studied, due to the fact that the stability of the DOB-based controllers for nonlinear systems has not been widely studied for robot control. It is of both theoretical and practical interests to investigate what capability can be achieved by developing the superiority of the combination of the disturbance observer and human operated control. In this paper, we propose a novel control mechanism combining robot automatic control and human operated control. The automatic control is realized on an exoskeleton robot using disturbance observer based adaptive control technique, while the human operated control is implemented by two steps: i) the stiffness of human operator arm is estimated from measured sEMG signals, based on the reported linear relationship between sEMG signals amplitude and end point force/stiffness; and ii) the real-time stiffness and damping are transferred from operator to the exoskeleton robot to implement human skills on the robot. Although various control methods on external disturbances attenuation are reported [11], [14], but very little efforts have been spent on the combination of the transferred impedance, adaptive control, and disturbance observer to realize disturbance rejection and impedance adaptation. Finally, we verified the effectiveness of our method through specific experiments.

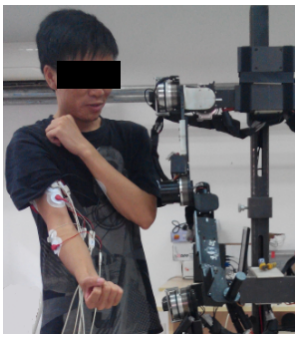

Fig. 1. The developed human robot coordination platform.

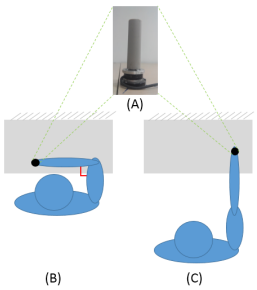

Fig. 2. (A) The force sensor used in the experiment. (B) and (C) are two required postures during the calibration.

II. System Description

A. Dynamics of Robots

The experimental platform under study is schematically shown in Fig. 1. In our experiment, the exoskeleton and the subject are teleoperated rather than physically coupled. The dynamics of an exoskeleton robot arm is same as that of an n-link rigid manipulator, and can be expressed by the Lagrange-Euler equation:

$$M(q)\ddot{q} + C(q,\dot{q})\dot{q} + G(q) + d(t) = B(q)\tau \qquad (1)$$

where $M(q) \in \mathbb{R}^{n\times n}$ is the symmetric bounded positive definite inertia matrix, $C(q,\dot{q})\dot{q} \in \mathbb{R}^n$ denote the Centripetal and Coriolis forces; $G(q) \in \mathbb{R}^n$ are the gravitational forces; $B(q) \in \mathbb{R}^{n\times r}$ is a full rank input transformation matrix and is assumed to be known because it is a function of the fixed geometry of the system; $\tau \in \mathbb{R}^r$ is the input torque vector; $d(t) \in \mathbb{R}^n$ is the disturbance vector; $q \in \mathbb{R}^n$.

Property 2.1: [15] The matrix M is symmetric and positive definite and the matrix $\dot{M} - 2C$ is skew-symmetric; and all Jacobian matrices are uniformly bounded and uniformly continuous if joint variable is uniformly bounded and continuous.

B. Cartesian Impedance Control on Stiffness Estimation Task

Operator's limb motion can be described either in operational space or in joint space. Similar to the actuation in human limb which is driven by muscles associated with related joint, the exoskeleton is also actuated by each motor attached to individual joint. Through focusing on the joint space, we can effectively avoid the redundancy problem in Cartesian space. Therefore, it can be easier to design controller directly in joint space. However, it is more convenient to specify impedance expressed in operational space to achieve the specified task. As a matter of fact, most of tasks are designed in operational space and the interactive forces are also defined in operational space, such that it is straightforward to calculate the force of external payload in operational space. Therefore, the transferred stiffness and damping will be transformed into the joint space, to be incorporated into the controller. The objective of this section is to estimate the limb stiffness by using the reported mapping between sEMG signals and end-effector forces/stiffness. In general, the desired compliance of the end-effector in operational space can be described in terms of a mechanical impedance, relating to the desired wrench response $F \in \mathbb{R}^6$ of the limb end-point (Fig. 2(A)) to a deviation $\Delta x \in \mathbb{R}^6$ from the desired position:

$$F = N\Delta\ddot{x} + D\Delta\dot{x} + K\Delta x \qquad (2)$$

where $N, D, K \in \mathbb{R}^{6\times 6}$ denote the desired inertia, viscosity and stiffness of the limb end-point, respectively [27], [28]. By choosing the desired inertia to the intrinsic inertia of the limb in its current state, the control objective (2) can be achieved without the need of force-feedback in the control loop with the following controls:

$$F = K\Delta x + D\Delta\dot{x} \qquad (3)$$

This article has been accepted for publication in a future issue of this journal, but has not been fully edited. Content may change prior to final publication. Citation information: DOI 10.1109/TIE.2016.2638403, IEEE Transactions on Industrial Electronics

where the end-point stiffness matrix K consists of four sub-matrices:

$$K = \begin{bmatrix} K_P & K_{PR} \\ K_{RP} & K_R \end{bmatrix} \quad (4)$$

with $K_P \in \mathbb{R}^{3\times3}$ relating forces to positional errors, $K_{PR} \in \mathbb{R}^{3\times3}$ relating forces to rotational errors, $K_{RP} \in \mathbb{R}^{3\times3}$ relating torques to positional errors and $K_R \in \mathbb{R}^{3\times3}$ relating torques to rotational errors. For simplicity, it can be practically assumed that $K_{PR} = K_{RP} = 0_{[3\times3]}$, which means that positional errors only result in force corrections, and rotational errors only result in torque corrections. Furthermore, the rotational stiffness can be written as K_R= diag($[K_R^x, K_R^y, K_R^z]$), where the diagonal elements represent the rotational stiffness around the three axes of the end-point frame of reference. The end-point viscosity D is designed to have the same structure as the end-point stiffness matrix:

$$D = \begin{bmatrix} D_P & 0 \\ 0 & D_R \end{bmatrix} \quad (5)$$

As shown in Fig. 2(B) (C), the human operator limb's force is measured by using the force sensor SRI-M3203 (Sunrise Instrument Co., Ltd) in the experiment. The rotation stiffness is translated as the arm moves [30], [31]. However, the rotational stiffness is unable to apply in the controller for the mechanical structure limitation of the exoskeleton robot. As result, the human operator will be restricted not to rotate hand in this study. The stiffness can be described as $K = K_P$ =diag$[K_{xx}, K_{yy}, K_{zz}]$, where the elements represent the stiffness on the three axes of the end-point frame of reference. The viscosity is described as $D = D_P$ =diag$[D_{xx}, D_{yy}, D_{zz}]$. In our case, the translational stiffness K_P is extracted from the sEMG signals and adaptive to the interaction force.

C. Simplification of Human Arm Stiffness

In [16], [17], [19], [20] and [32], it has been reported that the size of the endpoint stiffness ellipse can be changed after learning by the operator. This phenomenon can be interpreted as the property of central neural system (CNS) to adjust the stiffness of the joint in its equilibrium angle independent from the generated torque/force through the co-activation of agonistic/antagonistic muscle pairs. It is well known that sEMG signals are highly related to the static/dynamic stiffness and the skeletal muscle tensions. However, the relationship is nonlinear because of the nonlinear length and velocity dependency of the generated muscle tensions. Based on the fact that the sEMG signals are highly related to the static stiffness [21], and that the generated stiffness is highly related to the generated torque [16], [22], we assume the relationship is linear for the simplification and the moment arms are considered constant around the operational space in this paper. It shows that the correlation of rectified sEMG signals and force is approximately linear.

According to [17], [23], the linear relationship between sEMG signal amplitude and the end-point forces can be shown as:

$$f_{ej} = \sum_{i=1}^{m} \alpha_{i,j} \cdot A^{ago-i} - \sum_{i=1}^{m} \beta_{i,j} \cdot A^{anta-i} + r_j \quad (6)$$

where f_{ej} (j = x, y or z) denotes the generated forces at the human arm endpoint in x, y and z directions, respectively, m is the number of the pairs of the muscles in the experiments, and A^{anta-i} and A^{ago-i} are pre-processed antagonist/agonist sEMG signals and coefficients ($\alpha_{i,j}$, $\beta_{i,j}$) are all constants to be estimated, and r_x, r_y, r_z are the residual error caused by non-linear factors. In order to reduce residual error and simplify the complexity of experiment, incremental forces are introduced which can be expressed as

$$\Delta f_{ej} = \sum_{i=1}^{m} \alpha_{i,j} \cdot \Delta A^{ago-i} - \sum_{i=1}^{m} \beta_{i,j} \cdot \Delta A^{anta-i} + \Delta r_j \quad (7)$$

where $\Delta f_{ej} = f_{ej}(t+1) - f_{ej}(t)$ with ($j = x$, y or z) are incremental forces; $\Delta A^{ago-i} = A_{t+1}^{ago-i} - A_t^{ago-i}$; $\Delta A^{anta-i} = A_{t+1}^{anta-i} - A_t^{anta-i}$; $\Delta r_x = r_x(t+1) - r_x(t) \approx 0$, $\Delta r_y = r_y(t+1) - r_y(t) \approx 0$, $\Delta r_z = r_z(t+1) - r_z(t) \approx 0$, where t and $t+1$ are current and one step further sampling instants.

The mapping between limb end-point forces and sEMG signals of agonist/antagonist muscles is described by (6). It is well known that the muscle stiffness is approximately proportional to muscle torque [17], [18]. Therefore, the measurement of human arm end-point stiffness can be the total of the absolute values of numerous skeletal muscle torques. The specific stiffness estimation can be described as:

$$K_{jj} = \sum_{i=1}^{m} \mid \alpha_i \mid \cdot A^{ago-i} + \sum_{i=1}^{m} \mid \beta_i \mid \cdot A_t^{anta-i} + r_f^j \quad (8)$$

where K_{jj} with $j = x$, y or z denotes end-point stiffness of the human arm, and r_f^x, r_f^y, r_f^z denotes the non-linear residual errors. In this paper, a simplification model is adopted to estimate human arm incremental stiffness (9) to overcome possible non-linear residual items if the robot original stiffness is higher than the stiffness estimated from human muscle, some accidents may occur for the decrease of stiffness. So the calibration is necessary for the initialization of human robot interaction. Incremental stiffness estimation is introduced as:

$$\Delta K_{jj} = \sum_{i=1}^{m} \mid \alpha_i \mid \cdot \Delta A^{ago-i} + \sum_{i=1}^{m} \mid \beta_i \mid \cdot \Delta A^{anta-i} + \Delta r_f^j \quad (9)$$

where $\Delta K_{jj} = K_{jj}(t+1) - K_{jj}(t)$ with $j = x$, y or z are incremental stiffness; $\Delta A^{ago-i} = A_{t+1}^{ago-i} - A_t^{ago-i}$; $\Delta A^{anta-i} = A_{t+1}^{anta-i} - A_t^{anta-i}$; $\Delta r_f^x = r_f^x(t+1) - r_f^x(t) \approx 0$, $\Delta r_f^y = r_f^y(t+1) - r_f^y(t) \approx 0$, $\Delta r_f^z = r_f^z(t+1) - r_f^z(t) \approx 0$. The signal processing method used to detect instantaneous amplitude A_t^{ago-i} and A_t^{anta-i} will be detailed in section II-D. Finally, we can calculate stiffness matrix as follows:

$$K_P(t) = \text{diag}[K_{xx}(t), K_{yy}(t), K_{zz}(t)] \quad (10)$$

where $K_{jj}(t) = \sum_1^t \Delta K_{jj}$ with j = x, y or z. Although the above method would unavoidably bring precision and estimation errors, since relevant task is executed in the vicinity of the posture in which the related parameters are estimated, this method is still able to provide the intensive properties of the endpoint stiffness profile.

D. Stiffness Model Calibration

In order to calibrate the stiffness model which is described by (6) – (9), we perform a stiffness calibration as described below.

This article has been accepted for publication in a future issue of this journal, but has not been fully edited. Content may change prior to final publication. Citation information: DOI 10.1109/TIE.2016.2638403, IEEE Transactions on Industrial Electronics

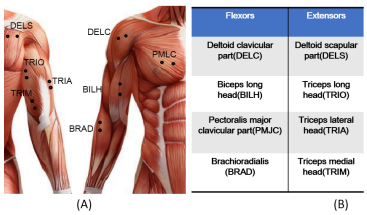

Flexors	Extensors
Deltoid clavicular part(DELC)	Deltoid scapular part(DELS)
Biceps long head(BILH)	Triceps long head(TRIO)
Pectoralis major clavicular part(PMJC)	Triceps lateral head(TRIA)
Brachioradialis (BRAD)	Triceps medial head(TRIM)

Fig. 3. A. Electrode positions in sEMG signals measurements. B. Information about these eight muscles. (This figure is modified from website: http://so.tooopen.com)

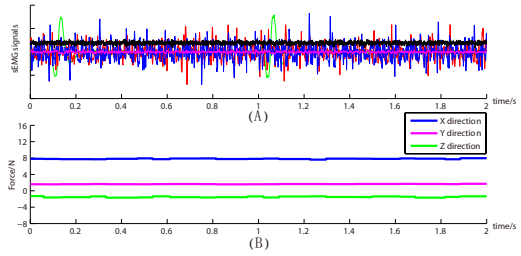

Fig. 4. (A)The extracted sEMG signals from eight electrodes; (B)The extracted force of x, y, z direction from the force sensors.

Three healthy human subjects (male, 52kg, 165 cm and 23 years (the thin representative); male, 58 kg, 169 cm and 24 years (the normal representative); male, 68kg, 173 cm and 25 years (the fat representative)) provided informed consent and participated in the experiment as operators. Each operator sits upright ahead of the cylindrical joint, which is designed for reducing undesired generated torques of the operators wrist. The joint is equipped with a 6 axis force-torque sensor (SRI-M3203). The required poses are presented in fig. 2. During each experiment, a real-time force data record in x, y, z direction was shown in Fig. 4. With visual feedback and isometric criteria, the operator was asked to apply the force or maintain the force at 4 N, 8 N, 12 N and 16 N along 4 directions [$\pm X$,$\pm Y$] and along the $\pm Z$ directions. More precisely, when the subjects applied forces to the force sensor in x/y/z direction, they are required to apply forces in specified directions while forces along other directions should as close to naught as possible. Each operator has to take this experiment 5 times for the estimation of the parameters in Eq. (6).

During experiment, sEMG data from eight muscles shown in Fig. 3(A) were obtained by using surface electrodes. The signals are sampled at 1024 Hz, bandpass filtered between 10 and 500 Hz, and notch filtered at 50 Hz. All the filters were implemented in software by employing Butterworth filtering technique. Furthermore, the maximum voluntary contraction (MVC) values are used to normalize to the extracted signals with the purpose of having extracted signals analogous to muscle activations. The end-point force and eight muscle activations are recorded during the experiments, and the parameters of (6) are estimated by means of least square-error approach with 72 trial data as results. Further, the absolute values of these parameters are used for the construction of co-contraction based index of endpoint stiffness profile as in (8).

We followed the above steps and calculated the parameters in (6) and Figs. 5, 6 and 7 show the estimated stiffness of end-point in X, Y, Z directions.

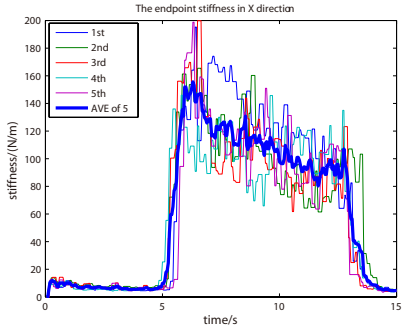

Fig. 5. The endpoint estimated stiffness of X direction.

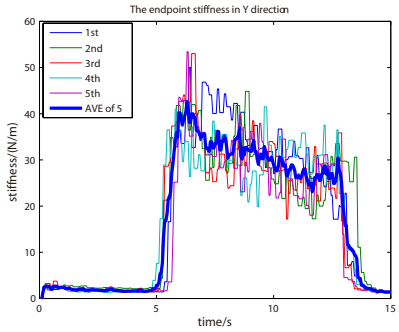

Fig. 6. The endpoint estimated stiffness of Y direction.

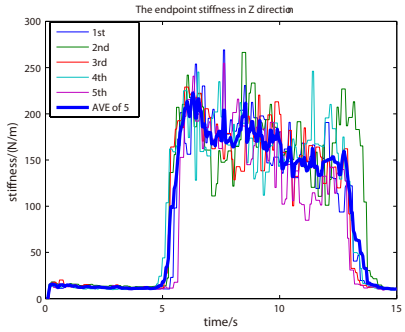

Fig. 7. The endpoint estimated stiffness of Z direction.

In Figs. 5, 6 and 7, the limb of operator is tightened during 5s-13s, and at the rest of time, the limb is on the relax situation. The pose of the limb of operator is required to be fixed. Further, in order to calculate the Jacobian matrix and get the joint stiffness, the specific motors in the arm of exoskeleton robot (shoulder and elbow) are set to move at sinusoidal trajectory (small-amplitude) without disturbance. We can see the obvious changes of end-point stiffness, since the blue thick line is the average stiffness during 5 times. After transformation, we can obtain the joint stiffness which are shown in Figs. 8 and 9.

Remark 2.1: The muscle length and moment arm variations are fairly smooth and bounded if the limits of the arm joint are not taken into account [32]. However, the length of wrist and elbow muscles changes by a small value in the middle ranges of

This article has been accepted for publication in a future issue of this journal, but has not been fully edited. Content may change prior to final publication. Citation information: DOI 10.1109/TIE.2016.2638403, IEEE Transactions on Industrial Electronics

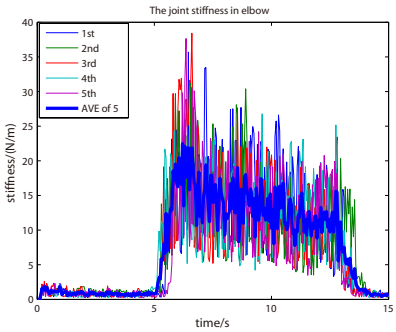

Fig. 8. Estimated stiffness of joint 1.

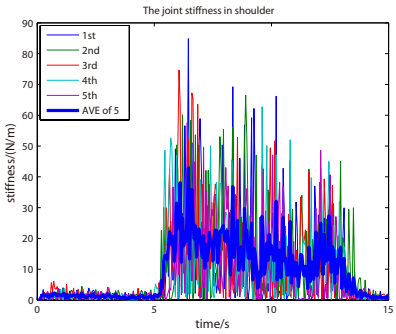

Fig. 9. Estimated stiffness of joint 2.

angular displacements [32], [33]. These remarks imply that in a certain volume of the human arm workspace, the character of arm geometry in directional variations of the Cartesian stiffness ellipsoid through Jacobian is more effective than the role of configuration-dependent joint stiffness term. Therefore, we can neglect the configuration-dependent effect of the joint stiffness matrix.

III. Biomimetic Impedance Control Design

The joint stiffness K_J can be estimated from sEMG signals by the calibration of the stiffness model, and then it will be incorporated into the disturbance observer based control system to be designed below. Let $e = q - q_d$, we can rewrite (1) as:

$$M(q)\ddot{e} + C(q,\dot{q})\dot{e} = u + \xi \tag{11}$$

with $u = B(q)\tau$, and $\xi = -M(q)\ddot{q}_d - C(q,\dot{q})\dot{q}_d - G(q) - d$.

Property 3.1: [39] There exist some finite positive constants $\alpha_i > 0$ and $\gamma_i > 0$, such that $\forall q_i \in \mathbb{R}^{n_i}$, $\|\xi_i\| \leq \alpha_i\|e_i\| + \gamma_i\|\dot{e}_i\|$.

Lemma 3.1: [24] For $x > 0$ and $\delta \geq 1$, we have $\ln(\cosh(x)) + \delta \geq x$.

Proof: If $x \geq 0$, one has $\int_0^x \frac{2}{e^{2s}+1}ds < \int_0^x \frac{2}{e^{2s}}ds = 1 - e^{-2x} < 1$, Therefore, $\ln(\cosh(x)) + \delta \geq \ln(\cosh(x)) + \int_0^x \frac{2}{e^{2s}+1}ds$ with $\delta \geq 1$. Let $f(x) = \ln(\cosh(x)) + \int_0^x \frac{2}{e^{2s}+1}ds - x$, one has $\frac{df(x)}{dx} = \tanh(x) + \frac{2}{e^{2x}+1} - 1 = \frac{e^x - e^{-x}}{e^x + e^{-x}} + \frac{2}{e^{2x}+1} - 1 = 0$. From the Mean Value Theorem [24], one has $f(x) - f(0) = \frac{df(x)}{dx}(x-0)$. Since $f(0) = 0$ and $\frac{df(x)}{dx} = 0$ for all x, one has $f(x) = 0$, that is, $\ln(\cosh(x)) + \int_0^x \frac{2}{e^{2s}+1}ds = x$, then, one has $\ln(\cosh(x)) + \delta \geq x$. ■

Remark 3.1: Consider Property 3.1 and Lemma 3.1, the upper bound of Φ_i satisfies

$$\|\Phi_i\| \leq \ln(\cosh(\|\Phi_i\|)) + \delta \tag{12}$$

where $\delta > 1$, $\Phi_i = \Lambda_i^T\varphi_i$ with $\varphi_i = [\|e_i\|, \|\dot{e}_i\|]^T$ and $\Lambda_i = [\alpha_i, \gamma_i]^T$ is a vector of positive constants being defined below.

For the ith row of (11), we have:

$$\sum_{j=1}^{n} m_{ij}\ddot{e}_j + \sum_{j=1}^{n} C_{ij}(q,\dot{q})\dot{e}_j = u_i + \xi_i \tag{13}$$

Since the dynamic uncertainty is one of the most important factors that could effect the control performance, we assume that actual value M can be divided as nominal part which denoted by $M^0 = \mathrm{diag}(m_1^0, \ldots, m_n^0)$ and uncertain part which denoted by $M - M^0$. Then in (11), we get the following vector-valued nominal linear system model with a disturbance term

$$M^0\ddot{e} = u + \omega \tag{14}$$

where M^0 is the nominal inertial diagonal matrix, and ω of same dimension is the disturbance vector defined as:

$$\omega = \xi - C(q,\dot{q})\dot{e} - (M(q) - M^0)\ddot{e} \tag{15}$$

Eq. (14) can be rewritten as:

$$m_i^0\ddot{e}_i = u_i + \omega_i \tag{16}$$

Because it is usually contaminated with high frequency noise while calculating $\ddot{e}_i$ by direct differentiation, a low-pass filter was set to pass ω_i through to obtain the estimate which is shown as:

$$Q_i(s)\omega_i = Q_i(s)(m_i^0 s\dot{e}_i - u_i) \tag{17}$$

where s denotes the Laplace operator and $Q_i(s) = \frac{1}{(1+\lambda_i s)^2}$, $\lambda_i > 0$. It is expected that $Q_i(s)\omega_i \approx \omega_i$ at low-frequencies due to limited pass-band of the disturbance observer (DOB). It is impossible to neglect the estimation error if the change of ω_i is fast. To simplify the analysis, a method [34] which saturates the outputs of DOB is proposed as:

$$\hat{\omega}_i = \begin{cases} \omega_i^- & \text{if } Q_i(s)(m_i^0 s\dot{e}_i - u_i) < \omega_i^- \\ Q_i(s)(m_i^0 s\dot{e}_i - u_i) & \text{if } \omega_i^- \leqslant Q_i(s)(m_i^0 s\dot{e}_i - u_i) \leqslant \omega_i^+ \\ \omega_i^+ & \text{else} \end{cases} \tag{18}$$

where ω_i^- and ω_i^+ are the selected lower and upper bound of ω_i.

Based on the disturbance observer (14), a control that incorporates human operator transferred impedance is presented as follows:

$$u_i = \nu_i - \hat{\omega}_i, \quad i = 1, 2, \ldots, n \tag{19}$$

$$\nu_i = -K_{Ji}e_i - D_{Ji}\dot{e}_i - \ln(\cosh(\hat{\Phi}_i))\mathrm{sgn}(\dot{e}_i) - \delta\mathrm{sgn}(\dot{e}_i) - \sigma|\hat{\omega}_i|\dot{e}_i \tag{20}$$

$$\dot{\hat{\alpha}}_i = -\rho_i\hat{\alpha}_i + \lambda_\alpha|e_i||\dot{e}_i| \tag{21}$$

$$\dot{\hat{\gamma}}_i = -\varrho_i\hat{\gamma}_i + \lambda_\gamma|\dot{e}_i|^2 \tag{22}$$

where $\hat{\Phi}_i = \hat{\Lambda}_i^T\varphi_i$ with $\varphi_i = [\|e_i\|, \|\dot{e}_i\|]^T$ and $\hat{\Lambda}_i = [\hat{\alpha}_i, \hat{\gamma}_i]^T$ is a vector of positive constants, $\rho_i > 0$ and $\varrho_i > 0$ satisfy $\lim_{t\to\infty}\rho_i = 0$ and $\lim_{t\to\infty}\varrho_i = 0$, $\lim_{t\to\infty}\int_0^t \rho_i(\varsigma)d\varsigma = a_i$

This article has been accepted for publication in a future issue of this journal, but has not been fully edited. Content may change prior to final publication. Citation information: DOI 10.1109/TIE.2016.2638403, IEEE Transactions on Industrial Electronics

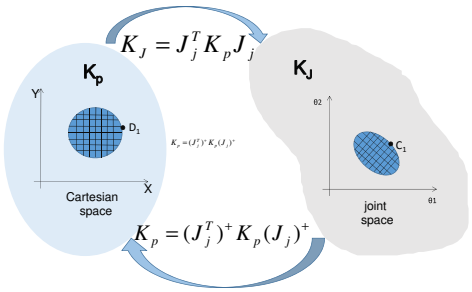

Fig. 10. The mapping between the operational space and the joint space.

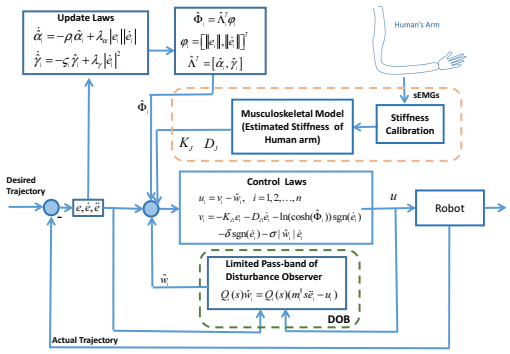

Fig. 11. The block diagram of the control design.

and $\lim_{t\to\infty}\int_0^t \varrho_i(\varsigma)d\varsigma = b_i$. $\hat{\omega}_i$ is the output of the disturbance observer, and $K_{Ji} > 0$, $D_{Ji} > 0$ are the transferred joint impedance from human operator. Let

$$K_J = \text{diag}[K_{J1}, \ldots, K_{Jn}], \quad D_J = \text{diag}[D_{J1}, \ldots, D_{Jn}] \quad (23)$$

and the joint stiffness K_J used in the control law of the exoskeleton robot is obtained by coordinate transformation from operational space by using Jacobian matrix J_j, i.e., $K_J = J_j^T K_P J_j$, where K_P is defined in (10), and is demonstrated in Fig. 10.

There are some works conducted to investigate the relationships between joint stiffness K_J and its viscosity D_J [16], [25], [26]. It is suggested that the damping ratio is constant regardless of co-contraction, which indicates a linear relationship between square root joint stiffness and the joint viscosity [16], [25], [26]. Therefore joint viscosity D_J of the control system can be presented as:

$$D_{Ji} = \varsigma\sqrt{K_{Ji}} \quad i = 1, \ldots, n \quad (24)$$

where the constant ς can be tuned to adjust the damping of the system.

Remark 3.2: In the block diagram of the controller shown in Fig. 11, the joint stiffness regulation from sEMG signals and the disturbance observer work together cooperatively. Disturbance observer allows us to reasonably estimate the external disturbances. When the external disturbance is slowly time varying, the performance of DOB is much better than its performance when the disturbance is in high frequency. Stiffness regulation is able to counteract the high frequency disturbance. When the stiffness levels of human arms are low, the main contribution of rejecting disturbances is the disturbance observer.

TABLE 1
THE EXPLANATION OF FOUR PHASES IN EXPERIMENT

	perturbation	perturbation kind(duration)	limb muscles
phase i	None	None	relax
phase ii	applied	low-frequency (≈1s)	relax
phase iii	applied	high-frequency (≈3s)	relax
phase iv	applied	high-frequency (≈3s)	stiffen up

Substituting (19) into (13) leads to the following closed-loop dynamics:

$$\sum_{j=1}^{n} m_{ij}\ddot{e}_j + \sum_{j=1}^{n} c_{ij}(q,\dot{q})\dot{e}_j = -K_{Ji}e_i - D_{Ji}\dot{e}_i - \delta\text{sgn}(\dot{e}_i) - \ln(\cosh(\hat{\Phi}_i))\text{sgn}(\dot{e}_i) - \sigma|\hat{\omega}_i|\dot{e}_i - \hat{\omega}_i + \xi_i \quad (25)$$

Theorem 3.1: Consider the mechanical system described by (1), using the control law (19), (20), (21) and (22), the following hold for any $(e_i(0), \dot{e}_i(0))$: e_i and $\dot{e}_i$ converge to a small set containing zero as $t \to \infty$; and τ are bounded for all $t \geq 0$.

The detailed proof is presented at the appendix section.

IV. EXPERIMENTS

A. Experimental Setup

To validate the effectiveness of the proposed method, the experiment is conducted in the presence of the external perturbations. The perturbations are applied at the joints of the manipulator in the opposite direction of the movement. The joints of robot are driven by the ELMO DC motor (Elmo Motion Control Ltd.). The overall schematic illustration of the experiment is shown in Fig. 12. Three layers which consist of human subject, the control unit and the exoskeleton robot are employed. By collecting the sEMG signals of human subject, the estimated stiffness is transferred to the control unit. The control unit collects data from stiffness estimator and disturbance observer, and then executes the control algorithms in real time to produce driving force to the DC motors. As shown in Fig. 13, the external perturbations in this experiment includes slow-frequency perturbation and high-frequency perturbation. The external perturbation would be only applied on the exoskeleton robot during the specified period as shown in Table 1.

Three healthy subjects, who have been involved in the experiment of stiffness model calibration at sec. II-D, have participated in this experiment section. At the beginning of the experiment, each subject is instructed to keep relax such that the stiffness transferred to the exoskeleton robot is small. In phase ii, the kind of external perturbation is of slow-frequency perturbation. A constant force is applied to the robot arm and then removed after about 1s. When the motors are on the balance situation for a while, the high-frequency perturbations are applied to the arm and then removed after about 3s (phase iii). It should be noticed that the muscle of the operator is relax in phase i, ii and iii. In phase iv, as a contrast to phase iii, the operator's arm stiffens up. Just as the same as phase iii, the

This article has been accepted for publication in a future issue of this journal, but has not been fully edited. Content may change prior to final publication. Citation information: DOI 10.1109/TIE.2016.2638403, IEEE Transactions on Industrial Electronics

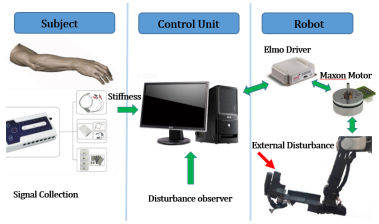

Fig. 12. The structure of system. It consists by three layers: human subject, control unit and the exoskeleton robot.

high-frequency perturbations are applied to the arm and then removed after about 3s.

The aim of the experimental design are: (1) when the transferred stiffness is low, the disturbance observer can effectively eliminate the slow-frequency perturbation but not good at dealing with the high-frequency perturbations. (2) the transferred stiffness can be changed by human operator obviously depending on the situation of muscles. (3) when the transferred stiffness is high (muscles of the operator stiffen up), the combination of the impedance transferring control and disturbance observer based automatic control can effectively eliminate the high-frequency perturbations.

As the robot has stiffness boundaries for the stable robot motion and the transferred stiffness varies from person to person, the modified stiffness of each subject is obtained by using the min-max normalization methods. In the experiment, the parameters employed in the control law are chosen as $\delta = 1.0$, $\lambda_\alpha = 0.01$, $\lambda_\gamma = 0.01$, $M^0 = \text{diag}[0.01, 0.01]$. Parameter σ is slightly different for different subjects. As shown in Table 1, the external disturbances are exerted at phase ii, iii and iv. In the experiments, no friction model is employed for friction compensation such that the nonlinear friction force proportional to the joint velocity, together with the uncertainties with joint mass of the joints will add into the internal disturbances, which are to be estimated and eliminated by using the disturbance observer.

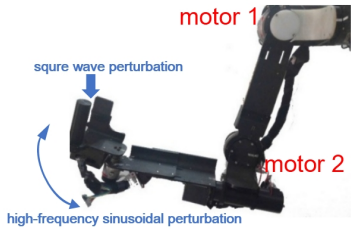

Fig. 13. The schematic figure of specific perturbation in this experiment. There are two kinds of perturbation : low-frequency perturbation and high-frequency perturbation.

B. Experimental Result and Analysis

The experimental results are shown in Figs. 14–16, which represent three subjects' performances. Fig. 14(A) (B), Fig. 15(A) (B) and Fig. 16(A) (B) show the estimated stiffness. The position error of joints of the exoskeleton robot are shown in Fig. 14(C) (D), Fig. 15(C) (D) and Fig. 16(C) (D). The performances of disturbance observer are shown in Fig. 14(E) (F), Fig. 15(E) (F) and Fig. 16(E) (F). The deep background colors are drawn to highlight the external perturbation in phase ii, iii and iv in the curves of position errors and estimated disturbances.

In phase i, all parameters are in the balance situation and no external perturbation is applied to the robot. It is the basis of the experiment. When the slow-frequency perturbation is applied at phase ii, the position error and estimated disturbance are changed obviously. When the perturbation is removed, the position error (Fig. 14(C) (D), Fig. 15(C) (D) and Fig. 16(C) (D)) comes back to the previous stages quickly for each motor. The estimated disturbance in Fig. 14(E) (F) become smooth quickly, and the estimated disturbance in Fig. 15(E) (F) and Fig. 16(E) (F) perform good and tend to the smooth situation. It is observed that the transferred stiffness of each motor is small in phase ii. It means that the disturbance observer can effectively eliminate the low-frequency perturbation when the transferred stiffness is small. This phenomenon verifies the effectiveness of the disturbance observer on dealing with the low-frequency perturbation.

In phase iii, the high-frequency perturbations are applied to the arm and then removed after about 3s. When the perturbations exist, the change frequency of position and the estimated disturbance is fast. When the high-frequency perturbations removed, position information in Fig. 14(C), Fig. 15(C) and Fig. 16(C) are not smooth. Fig. 14(D), Fig. 15(D) and Fig. 16(D) tend to become smooth. However, the estimated disturbances in Fig. 15(E) (F) and Fig. 16(E) (F) are not smooth and the curves are turbulent.

In contrast to phase iii, phase iv has all the same situation of phase iii but the difference of transferred stiffness. At this phase, the muscles of the subject's limb stiffen up. The amplitude differences of transferred stiffness between phase iii and phase iv in Fig. 14(A) (B), Fig. 15(A) (B) and Fig. 16(A) (B) are obvious. For different subject, the shape and the amplitude of the transferred stiffness in phase iv are different. When the dynamic high-frequency perturbations removed, the change frequency of position, estimated information is still fast. After a little while, it is observed that the position error become smooth. Furthermore, the estimated disturbances are also smooth. Compared phase iii to phase iv in Fig. 14(E) (F), Fig. 15(E) (F) and Fig. 16(E) (F), the effectiveness of the transferred stiffness is obvious. This phenomenon verifies the effectiveness of the combination of the impedance transferring control and disturbance observer based automatic control on eliminating the high-frequency bounded perturbations.

V. Conclusions

In this paper, a control method combining the human stiffness transfer and adaptive control techniques and the disturbance observer has been constructed to maintain stability and to eliminate the effect of external perturbations. The proposed controller is robust to both system model uncertainties and external disturbances. Experimental studies have been conducted to verify the effectiveness of the proposed method. The control method developed in this paper has a great potential application in telerobot manipulation and robot assistive rehabilitation. The paper proposed the approach applied in the human-robot

This article has been accepted for publication in a future issue of this journal, but has not been fully edited. Content may change prior to final publication. Citation information: DOI 10.1109/TIE.2016.2638403, IEEE Transactions on Industrial Electronics

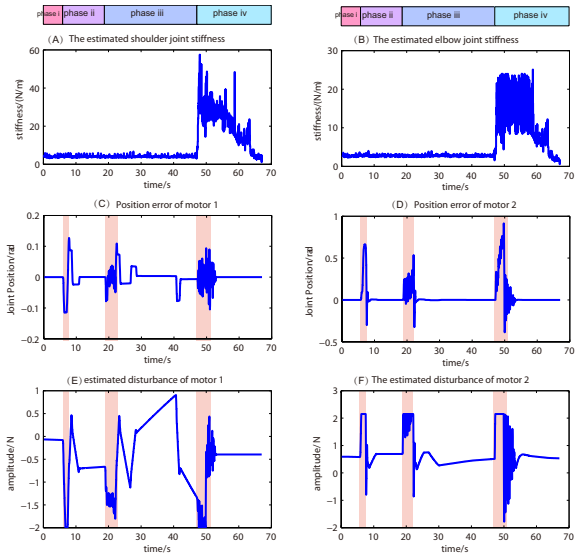

Fig. 14. The experimental results of subject P1. (A) and (B) represent the curve of estimated joint stiffness; (C) and (D) represent the curve of motor position errors; (E) and (F) represent the curve of estimated disturbances. The deep background colors are drawn to highlight the external perturbation in phase ii, iii and iv of (C),(D),(E) and (F).

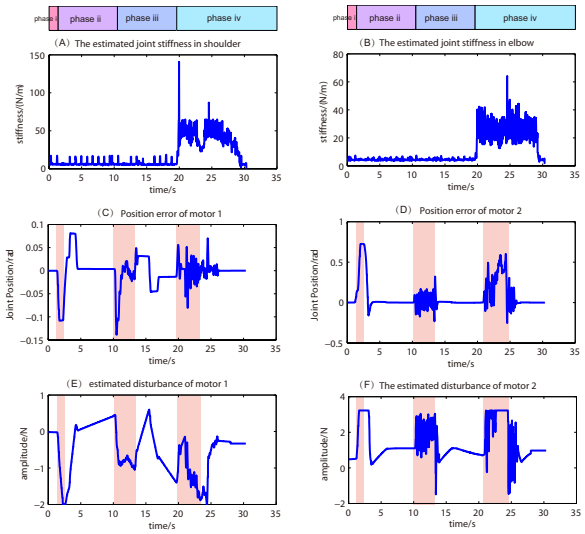

Fig. 15. The experimental results of subject P2. (A) and (B) represent the curves of estimated joint stiffness; (C) and (D) represent the curves of motor position errors; (E) and (F) represent the curves of estimated disturbances. The deep background colors are drawn to highlight the external perturbation in phase ii, iii and iv of (C),(D),(E) and (F).

teleoperation scenario, we consider that the exoskeleton robot is tele-operated by the operator, and both are not physically coupled, where the human arm was outside of the robotic arm. In future work, we shall consider physically human-robot coupled scenario, where human and robot limbs are usually tightly physically coupled therefore the dynamics and control are significantly different. If the exoskeleton is physically coupled with the human arm, the muscle activity patterns in the human arm need to be recognized by cognitive computation and signal processing, it can provide the reference motion/position for the exoskeleton control.

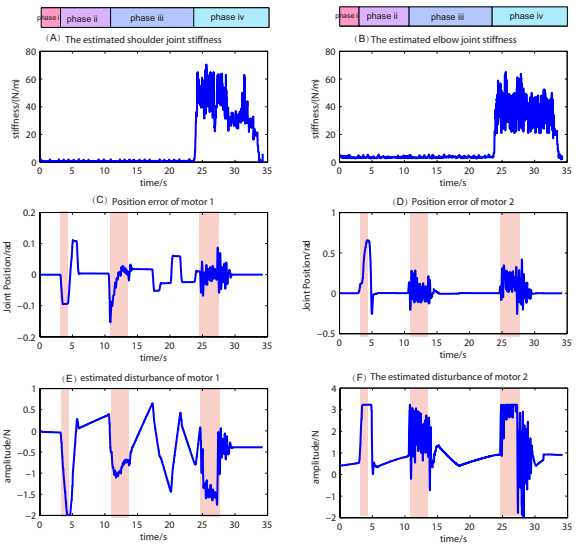

Fig. 16. The experimental results of subject P3. (A) and (B) represent the curve of estimated joint stiffness; (C) and (D) represent the curve of motor position errors; (E) and (F) represent the curve of estimated disturbances. The deep background colors are drawn to highlight the external perturbation in phase ii, iii and iv of (C),(D),(E) and (F).

VI. Appendix

Proof: To facilitate the control design, consider the following Lyapunov function with $\tilde{\alpha}_i = \alpha_i - \hat{\alpha}_i$ and $\tilde{\gamma}_i = \gamma_i - \hat{\gamma}_i$ as

$$V = \frac{1}{2}e^T K_J e + \frac{1}{2}\dot{e}^T M \dot{e} + \frac{1}{2\lambda_\alpha}\tilde{\alpha}^2 + \frac{1}{2\lambda_\gamma}\tilde{\gamma}^2 \quad (26)$$

The derivative of V along (26) is given as

$$\begin{aligned}\dot{V} &= e^T K_J \dot{e} + \sum_{k=1}^{n}\left(\frac{1}{\lambda_\alpha}\dot{\tilde{\alpha}}_k\tilde{\alpha}_k + \frac{1}{\lambda_\gamma}\dot{\tilde{\gamma}}_k\tilde{\gamma}_k\right) \\ &\quad + \frac{1}{2}\left[\dot{e}^T\dot{M}\dot{e} + \ddot{e}^T M\dot{e} + \dot{e}^T M\ddot{e}\right] \\ &= \sum_{k=1}^{n} K_{Jk}e_k\dot{e}_k + \sum_{k=1}^{n}\left(\frac{1}{\lambda_\alpha}\dot{\tilde{\alpha}}_k\tilde{\alpha}_k + \frac{1}{\lambda_\gamma}\dot{\tilde{\gamma}}_k\tilde{\gamma}_k\right) \\ &\quad + \sum_{i=1}^{n}\dot{e}_i\left[\frac{1}{2}\sum_{j=1}^{n}\dot{m}_{ij}\dot{e}_j + \sum_{j=1}^{n} m_{ij}\ddot{e}_j\right] \end{aligned} \quad (27)$$

Substituting (13) into (27), we get

$$\begin{aligned}\dot{V} &= \sum_{k=1}^{n} K_{Jk}e_k\dot{e}_k + \sum_{k=1}^{n}\left(\frac{1}{\lambda_\alpha}\dot{\tilde{\alpha}}_k\tilde{\alpha}_k + \frac{1}{\lambda_\gamma}\dot{\tilde{\gamma}}_k\tilde{\gamma}_k\right) \\ &\quad + \sum_{i=1}^{n}\dot{e}_i\left[\frac{1}{2}\sum_{j=1}^{n}\dot{m}_{ij}\dot{e}_j - \sum_{j=1}^{n} C_{ij}\dot{e}_j + u_i + \xi_i\right] \end{aligned} \quad (28)$$

Considering Property 2.1, and integrating (19) into (28), we have

$$\begin{aligned}\dot{V} &= \sum_{k=1}^{n} K_{Jk}e_k\dot{e}_k + \sum_{i=1}^{n}\dot{e}_i(u_i+\xi_i) \\ &\quad + \sum_{k=1}^{n}\frac{1}{\lambda_\alpha}\dot{\tilde{\alpha}}_k\tilde{\alpha}_k + \sum_{k=1}^{n}\frac{1}{\lambda_\gamma}\dot{\tilde{\gamma}}_k\tilde{\gamma}_k \\ &= \sum_{k=1}^{n} K_{Jk}e_k\dot{e}_k + \sum_{k=1}^{n}\dot{e}_k[-K_{Jk}e_k - D_{Jk}\dot{e}_k \\ &\quad -\sigma|\hat{\omega}_k|\dot{e}_k - \hat{\omega}_k - \ln(\cosh(\hat{\Phi}_k))\mathrm{sgn}(\dot{e}_k) \\ &\quad -\delta\mathrm{sgn}(\dot{e}_k) + \xi_k] + \sum_{k=1}^{n}(\frac{1}{\lambda_\alpha}\dot{\tilde{\alpha}}_k\tilde{\alpha}_k + \frac{1}{\lambda_\gamma}\dot{\tilde{\gamma}}_k\tilde{\gamma}_k) \\ &= -\sum_{k=1}^{n} D_{Jk}\dot{e}_k^2 - \sum_{k=1}^{n}(\ln(\cosh(\hat{\Phi}_k)) + \delta)|\dot{e}_k| \\ &\quad -\sum_{k=1}^{n}|\hat{\omega}_k|(\sqrt{\sigma}|\dot{e}_k| + \frac{1}{2\sqrt{\sigma}})^2 + \sum_{k=1}^{n}\frac{|\hat{\omega}_k|}{4\sigma} \\ &\quad + \sum_{k=1}^{n}\dot{e}_k\xi_k + (\sum_{k=1}^{n}\frac{1}{\lambda_\alpha}\dot{\tilde{\alpha}}_k\tilde{\alpha}_k + \sum_{k=1}^{n}\frac{1}{\lambda_\gamma}\dot{\tilde{\gamma}}_k\tilde{\gamma}_k)\end{aligned} \tag{29}$$

Considering Lemma 3.1 and (18), we get

$$\begin{aligned}\dot{V} &\le -\sum_{k=1}^{n} D_{Jk}\dot{e}_k^2 + \sum_{k=1}^{n}\dot{e}_k\xi_k + \sum_{k=1}^{n}\frac{\omega_k^+}{4\sigma} \\ &\quad -\sum_{k=1}^{n}\hat{\alpha}_k\|\dot{e}_k\|\|e_k\| - \sum_{k=1}^{n}\hat{\gamma}_k\|\dot{e}_k\|^2 \\ &\quad + \sum_{k=1}^{n}(\frac{1}{\lambda_\alpha}\dot{\tilde{\alpha}}_k\tilde{\alpha}_k + \frac{1}{\lambda_\gamma}\dot{\tilde{\gamma}}_k\tilde{\gamma}_k)\end{aligned} \tag{30}$$

Considering Property 3.1, we have $\sum_{k=1}^{n}\dot{e}_k\xi_k \le \sum_{k=1}^{n}(\alpha_k|e_k||\dot{e}_k| + \gamma_k|\dot{e}_k|^2)$. Considering $\tilde{\alpha}_k = \alpha_k - \hat{\alpha}_k$, its derivative $\dot{\tilde{\alpha}}_k = -\dot{\hat{\alpha}}_k$, and the adaptive law (21), we have $\frac{1}{\lambda_\alpha}\dot{\tilde{\alpha}}_k\tilde{\alpha}_k = \frac{\rho_k}{\lambda_\alpha}\hat{\alpha}_k\tilde{\alpha}_k - \tilde{\alpha}_k|e_k||\dot{e}_k|$. Considering $\tilde{\gamma}_k = \gamma_k - \hat{\gamma}_k$, its derivative $\dot{\tilde{\gamma}}_k = -\dot{\hat{\gamma}}_k$, and the adaptive law (22), we have $\frac{1}{\lambda_\gamma}\dot{\tilde{\gamma}}_k\tilde{\gamma}_k = \frac{\varrho_k}{\lambda_\gamma}\hat{\gamma}_k\tilde{\gamma}_k - \tilde{\gamma}_k|\dot{e}_k|^2$. Integrating the above equations into (30), we can obtain

$$\begin{aligned}\dot{V} &\le -\sum_{k=1}^{n} D_{Jk}\dot{e}_k^2 + \sum_{k=1}^{n}\frac{\omega_k^+}{4\sigma} + \sum_{k=1}^{n}(\frac{\rho_k}{\lambda_\alpha}\hat{\alpha}_k\tilde{\alpha}_k + \frac{\varrho_k}{\lambda_\gamma}\hat{\gamma}_k\tilde{\gamma}_k) \\ &\le -\sum_{k=1}^{n} D_{Jk}\dot{e}_k^2 + \frac{1}{4}\sum_{k=1}^{n}(\frac{\omega_k^+}{\sigma} + \frac{\rho_k}{\lambda_\alpha}\alpha_k^2 + \frac{\varrho_k}{\lambda_\gamma}\gamma_k^2)\end{aligned} \tag{31}$$

Let $\Delta = \frac{1}{4}\sum_{k=1}^{n}(\frac{\omega_k^+}{\sigma} + \frac{\rho_k}{\lambda_\alpha}\alpha_k^2 + \frac{\varrho_k}{\lambda_\gamma}\gamma_k^2)$. As ω_k^+ and σ are constants and $t \to \infty$ by noting $\lim_{t\to\infty}\rho_k = 0$ and $\lim_{t\to\infty}\varrho_k = 0$, Δ is bounded and converges to zero. There exists $t > t_1$, Δ with a finite small constant ϖ, when $|\dot{e}_k| \ge \sqrt{\frac{\varpi}{\lambda_{min}(D_{Jk})}}$, $\dot{V} \le 0$. From above all, $\dot{e}_k$ converges to a small set containing the origin as $t \to \infty$.

Integrating both sides of the above equation gives $V(t) - V(0) < \int_0^t[-\sum_{k=1}^{n} D_{Jk}\dot{e}_k^2 + \sum_{k=1}^{n}\frac{\omega_k^+}{4\sigma} + \frac{1}{4}\sum_{k=1}^{n}(\frac{\rho_k}{\lambda_\alpha}\alpha_k^2 + \frac{\varrho_k}{\lambda_\gamma}\gamma_k^2)]$ by noting $\lim_{t\to\infty}\rho_k = 0$ and $\lim_{t\to\infty}\varrho_k = 0$. Thus V is bounded, which implies that $e, \dot{e} \in L_\infty$. As we have established $e, \dot{e} \in L_\infty$, we conclude that $u, \dot{u} \in L_\infty$. Therefore, all the signals on the right hand side of (13) are bounded, and it is easy to conclude that u_i is bounded from (19).

REFERENCES

[1] Y. Ueyama and E. Miyashita, "Optimal feedback control for predicting dynamic stiffness during arm movement," *IEEE Trans. Ind. Electron.*, vol. 61, no. 2, pp. 1044-1052, Feb. 2014.

[2] Z. Li, C. Yang, and E. Burdet, "An overview of biomedical robotics and bio-mechatronics systems and applications," *IEEE Trans. Systems Man and Cybernetics: Systems*, vol. 46, no. 7, pp. 869–874, July 2016.

[3] X. Zhao, Y. Chu, J. Han, Z. Zhang, "SSVEP-based brain-computer interface controlled functional electrical stimulation system for upper extremity rehabilitation,"*IEEE Trans. Systems Man and Cybernetics: Systems*, vol. 46, no. 7, pp. 947–956, July 2016.

[4] E. Burdet, R. Osu, D. Franklin, T. E. Milner, and M. Kawato, "The central nervous system stabilizes unstable dynamics by learning optimal impedance," *Nature*, vol. 414, no. 6862, pp. 446-449, 2001.

[5] J.-S. Hu, J.-J. Wang, and D. M. Ho, "Design of sensing system and anticipative behavior for human following of mobile robots," *IEEE Trans. Ind. Electron.*, vol. 61, no. 4, pp. 1916-1927, Apr. 2014.

[6] A. Albu-Schaffer, S. Haddadin, C. Ott, A. Stemmer, T. Wimbock, and G. Hirzinger, "The DLR lightweight robot: design and control concepts for robots in human environments," *Ind. Robot.*, vol. 34, no. 5, pp. 376-385, 2007.

[7] G. Berselli, A. Guerra, G. Vassura, A. O. Andrisano, "An engineering method for comparing selectively compliant joints in robotic structures," *IEEE/ASME Trans. Mechatronics*, vol. 19, no. 6, pp. 1882-1895, Dec. 2014.

[8] C. Sun, W. L. Xu, J. E. Bronlund, and M. Morgenstern, "Dynamics and compliance control of a linkage robot for food chewing," *IEEE Trans. Ind. Electron.*, vol. 61, no. 1, pp. 377-386, Jan. 2014.

[9] Z. Li, C. Yang, Y. Tang, "Decentralised adaptive fuzzy control of coordinated multiple mobile manipulators interacting with non-rigid environments," *IET Control Theory & Applications*, vol. 7, no. 3, pp. 397-410, 2013.

[10] A. Ajoudani, N. G. Tsagarakis, A. Bicchi, "Tele-impedance: teleoperation with impedance regulation using a body-machine interface," *The International Journal of Robotics Research*, vol. 31, no. 13, pp. 1642-1656, 2014.

[11] M. Chen, S. Ge, "Direct adaptive neural control for a class of uncertain nonaffine nonlinear systems based on disturbance observer," *IEEE Trans. Cybernetics*, vol. 43, no. 4, pp. 1213-1225, Aug. 2013.

[12] D. Ginoya, P. D. Shendge, and S. B. Phadke, "Sliding mode control for mismatched uncertain systems using an extended disturbance observer," *IEEE Trans. Ind. Electron.*, vol. 61, no. 4, pp. 1983-1992, Apr. 2014.

[13] Z. J. Yang, H. Tsubakihara, S. Kanae, K.Wada, and C.-Y. Su, "A novel robust nonlinear motion controller with disturbance observer,"*IEEE Trans. Control Systems Technology*, vol. 16, no. 1, pp. 137-147, Jan. 2008.

[14] M. W. Vandegrift, F. L. Lewis, S. Q. Zhu, "Flexible-link robot arm control by a feedback linearization/singular perturbation approach," *Journal of Robotic Systems*, pp. 591-603, 1994.

[15] L. Sciavicco, L. Villani, "Robotics: modelling, planning and control", *Springer*, 2009.

[16] H. Gomi and R. Osu, "Task-dependent viscoelasticity of human multijoint arm and its spatial characteristics for interaction with environments,"*Journal of Neuroscience*, vol. 18, pp. 8965-8978, 1998.

[17] R. Osu, D. W. Franklin, H. Kato, H. Gomi, K. Domen, T. Yoshioka, and M. Kawato, "Short- and long-term changes in joint co-contraction associated with motor learning as revealed from surface emg," *Journal of Neurophysiology*, vol. 88, no. 5, pp. 991-1004, 2002.

[18] A. Ajoudani, N. G. Tsagarakis, and A. Bicchi, "Tele-impedance: Preliminary results on measuring and replicating human arm impedance in tele operated robots,"*IEEE International Conference of Robotics and Biomimetics (ROBIO)*, 2011, pp. 216-222.

[19] J. M. Dolan, M. B. Friedman, M. L. Nagurka, "Dynamic and loaded impedance components in the maintenance of human arm posture," *IEEE Trans. Systems. Man. Cybern.*, vol. 23, pp. 698-709, May/Jun. 1993.

[20] T. Tsuji, P. G. Morasso, K. Goto, and K. Ito, "Human hand impedance characteristics during maintained posture," *Biological Cybernetics*, vol. 72, pp.475-485, 1995.

[21] R. Osu and H. Gomi, "Multi-joint muscle regulation mechanisms examined by measured human-arm stiffness and EMG signals," *Journal of Neurophysiology*, vol. 81, pp. 1458-1468, 1999.

[22] I. Hunter and R. Kearney, "Dynamics of human ankle stiffness: variation with mean ankle torque," *Journal of Biomechanics*, vol. 15, pp. 747-752, 1982.

[23] P. Liang, C. Yang, N. Wang, Z. Li, R. Li, E. Burdet, "Implementation and test of human-operated and human-like adaptive impedance controls on baxter robot," *Advances in Autonomous Robotics Systems*, pp. 109-119, 2014.
[24] Z. Li, C. Yang, L. Fan, *Advanced control of wheeled inverted pendulum systems*, Springer , 2013.
[25] F. Lacquaniti, F. Licata, J. F. Soeching, "The mechanical behavior of the human forearm in response to transient perturbation," *Biological Cybernetics*, vol. 44, pp. 35-46, 1982.
[26] R. E. Kearney, I. W. Hunter, "System identification of human joint dynamics," *Critical Reviews in Biomedical Engineering*, vol. 18, pp. 55-87, 1989.
[27] N. Hogan "Impedance control: An approach to manipulation", *IEEE American Control Conference*, pp. 304-313, 1984.
[28] K. Kronander, A. Billard, "Learning compliant manipulation through kinesthetic and tactile human-robot interaction," *IEEE Trans. on Haptics*, vol. 27, no. 5, pp. 367-380, July-Sept. 2014.
[29] K. Ohnishi, M. Shibata, T. Murakami, "Motion control for advanced mechatronics," *IEEE/ASME Trans. on Mechatronics*, vol. 1, no. 1, pp. 56-67, Mar 1996.
[30] M. Stokdijk, J. Nagels, P. M. Rozing, "The glenohumeral joint rotation centre in vivo," *Journal of Biomechanics*, vol. 33, pp. 1629-1636, Dec. 2000.
[31] M. A. Ergin, V. Patoglu, "ASSISTON-SE: A self-aligning shoulder-elbow exoskeleton," *IEEE International Conference Robotics and Automation*, pp. 2479-2485, May 2012.
[32] P. Pigeon, L. H. Yahia, A. G. Feldman, "Moment arms and lengths of human upper limb muscles as functions of joint angles." *Journal of Biomechanics*, vol. 29, no. 10, pp. 1365-1370, 1996.
[33] A. Ajoudani, C. Fang, N. G. Tsagarakis, A. Bicchi, "A reduced-complexity description of arm endpoint stiffness with applications to teleimpedance control." *2015 IEEE/RSJ International Conference on Intelligent Robots and Systems (IROS)*, 2015, pp. 1017-1023.
[34] Z. Yang, Y. Fukushima, P. Qin, "Decentralized adaptive robust control of robot manipulators using disturbance observers, " *IEEE Trans. Control Systems Technology*, vol. 20, no. 5, pp. 1357–1365, Sept. 2012.
[35] W. He, Y. Dong, C. Sun, "Adaptive neural impedance control of a robotic manipulator with input saturation, " *IEEE Trans. Systems, Man, and Cybernetics: Systems*, vol. 46, no. 3, pp. 334–344, Mar. 2016.
[36] H. Modares, I. Ranatunga, F. L. Lewis, D. O. Popa, "Optimized assistive humanCrobot interaction using reinforcement learning, " *IEEE Trans. Cybernetics*, vol. 46, no. 3, pp. 655–667, March 2016.
[37] H. Xiao, Z. Li, C. L. P. Chen, "Formation Control of leader-follower mobile robots systems using model predictive control based on neural-dynamic optimization, " *IEEE Trans. Ind. Electron.*, vol. 63, no. 9, pp. 5752–5762, Sept. 2016.
[38] J. E. Slotine, W. Li, *Applied nonlinear control*, NJ: Prentice-Hall, 1991.
[39] S. Hsu, L. Fu, "A fully adaptive decentralized control of robot manipulators," *Automatica*, vol. 42, pp. 1761-1767, Oct. 2006.

Zhijun Li (M'07-SM'09) received the Ph.D. degree in mechatronics, Shanghai Jiao Tong University, P. R. China, in 2002. From 2003 to 2005, he was a postdoctoral fellow in Department of Mechanical Engineering and Intelligent systems, The University of Electro-Communications, Tokyo, Japan. From 2005 to 2006, he was a research fellow in the Department of Electrical and Computer Engineering, National University of Singapore, and Nanyang Technological University, Singapore. From 2007-2011, he was an Associate Professor in the Department of Automation, Shanghai Jiao Tong University, P. R. China. Since 2012, he is a Professor in College of Automation Science and Engineering, South China university of Technology, Guangzhou, China.

From 2016, he has been the Chair of Technical Committee on Biomechatronics and Biorobotics Systems (B^2S), IEEE Systems, Man and Cybernetics Society. He is serving as an Editor-at-large of Journal of Intelligent & Robotic Systems, and Associate Editors of several IEEE Transactions. He has been the General Chair of 2016 IEEE Conference on Advanced Robotics and Mechatronics, Macau, China. Dr. Li's current research interests include service robotics, tele-operation systems, nonlinear control, neural network optimization, etc.

Yu Kang (M'09-SM'14) received the Dr.Eng. degree in control theory and control engineering from the University of Science and Technology of China, Hefei, China, in 2005. From 2005 to 2007, he was a Post-Doctoral Fellow with the Academy of Mathematics and Systems Science, Chinese Academy of Sciences, Beijing, China. He is currently a Professor with the Department of Automation, and with the State Key Laboratory of Fire Science, and with the Institute of Advanced Technology, University of Science and Technology of China. His current research interests include adaptive/robust control, variable structure control, mobile manipulator, and Markovian jump systems.

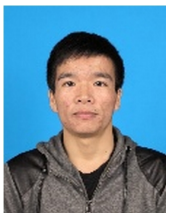

Zhiye Xiao received the B.Eng. degree in College of Automation Science and Engineering, South China Univ. of Tech., Guangzhou, China, in 2013. He is working toward Master Degree in in College of Automation Science and Engineering, South China Univ. of Technology. His research interests are exoskeleton robot, bio-signal processing.

Weiguo Song is the professor of the State Key Laboratory of Fire Science, University of Science and Technology of China(USTC). He received bachelor degree and Ph.D degree of Engineering Thermal Physicsat from the University of Science and Technology of China, in 1996 and 2001. He worked as a postdoc fellowin USTC from 2001 to 2003, and as a guest researcher at NIST from 2006 to 2007. He has authored over 60 research papers that published in Fire safety Journal, IEEE-ITS, Safety Science, Building and Environment and other international journals. He has chaired international conferences such as PED2016, and acted as session chairs or committee members in IAFSS, PED, TGF conferences. He won the National Prize for Progress in Science and Technology of China, China Youth Science and Technology Award and some other awards. His research areas include Pedestrian and evacuation dynamics, complex system, Performance-based fire protection design, Fire monitoring with remote sensing.